Electronic Supporting Information

Ion and Hole Dual-Channel Transport Columnar Mesomorphic Organic Electronic Materials with High Anisotropic Conductivities Based on Supramolecular Discotic Ionic Liquid Crystals

Jian Chen,[‡a] Yuhao Sun,[‡a] Weiguang Zhao,[a] Jiang Liu,[a] Jianglin Fang,[b] Tianchi Xu *[a] and Dongzhong Chen*[a]

[a]Key Laboratory of High Performance Polymer Materials and Technology of Ministry of Education, Collaborative Innovation Center of Chemistry for Life Sciences, Department of Polymer Science and Engineering, School of Chemistry and Chemical Engineering, Nanjing University, Nanjing 210023 (China), E-mail: cdz@nju.edu.cn, xtc@nju.edu.cn

[b]Center for Materials Analysis, Nanjing University, Nanjing 210093 (China)

‡ These authors contributed equally to this work.

Table of contents

1. Reagents, synthesis and characterization of building blocks

Benzo-18-Crown-6 (97%, J&K), 1,2,3-trihydroxybenzene (85%, TCI) 1-bromooctane (98%, TCI), 1-bromodecane (98%, TCI), 1-bromododecane (97%, TCI), 1-bromotetradecane (97%, TCI), 1-bromohexadecane (97%, TCI), cation exchange resin IR120 (AR, Nanjing Chemical Reagent Co. Ltd.) were used as received. All solvents were dried and distilled before use. All other chemical reagents were commercially available and used as received. Al_2O_3 ceramic-based interdigital electrodes (finger width 35 μm, finger spacing 35 μm, surface Au thickness 1.0 μm, inner Cu thickness 4.0 μm, electrode number 10 pairs, maximum working temperature 250 ℃) were purchased form Yuxin Co. Ltd.

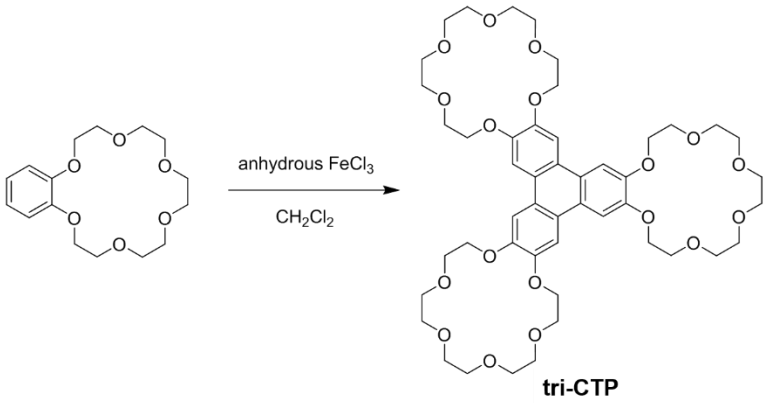

Scheme S1 Synthesis of tris(18-crown-6)triphenylene (**tri-CTP**) through trimerization in the presence of $FeCl_3$.

The synthesis of tris(18-crown-6)triphenylene (**tri-CTP**) (Scheme S1) was carried out through trimerization of benzo-18-crown-6 via catalytic oxidation with anhydrous $FeCl_3$ in a rather high yield around 70% as described in detail in our previous reported procedure.[1]

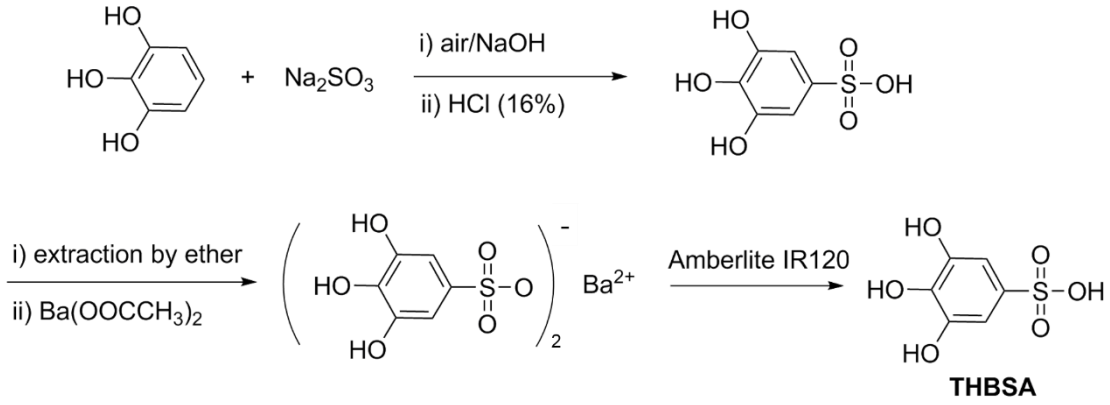

Scheme S2 Synthesis route for 3,4,5-trihydroxybenzenesulfonic acid (THBSA).

3,4,5-trihydroxybenzenesulfonic acid: As shown in Scheme S2, the synthesis of 3,4,5-trihydroxybenzenesulfonic acid (THBSA) was carried out according to the literature procedure.[2] Into a 100 mL aqueous solution of pyrogallol (10.00 g, 0.08 mol), Na_2SO_3 (24.10 g, 0.19 mol) and NaOH (3.34 g, 0.08 mol), air was continuously blown over a period of 6 h. The obtained brown reaction solution was acidified with 40 mL HCl solution (16%) and was repeatedly extracted (10 times at least) with diethyl ether to remove the residual starting materials. From this pre-purified aqueous solution, all SO_3^{2-} ions were removed by adding barium acetate solution (48.84 g, 0.19 mol). Subsequently, the filtrate was run over an ion-exchange column (Amberlite IR120) to remove any residual metal ions. White solids were separated upon evaporation of water under vacuum. The crude product was dried under vacuum for 48 h to produce 8.70 g of crystalline solid product 3,4,5-trihydroxybenzenesulfonic acid (yield: 53%). ^{1}H NMR (400 MHz, D_2O) δ 6.84 (s, 2H).

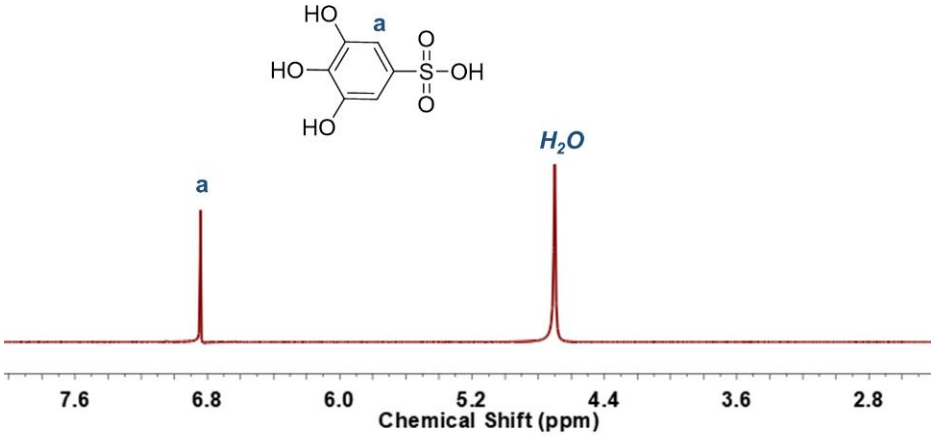

Fig. S1 ^{1}H NMR spectrum in D_2O of the synthesized 3,4,5-trihydroxybenzenesulfonic acid (THBSA).

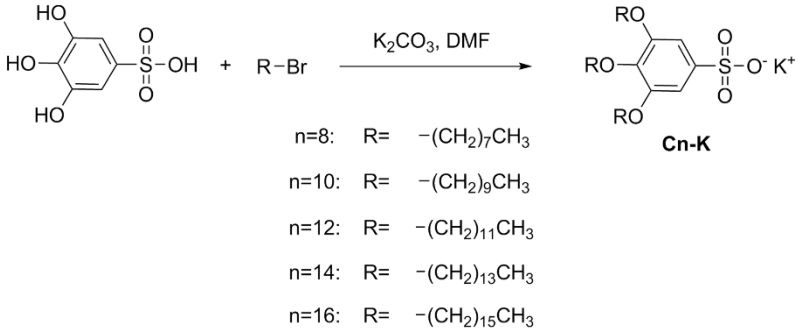

Scheme S3 Schematic synthesis route for potassium 3,4,5-trialkoxybenzenesulfonates Cn-K (alkyl carbon number n = 8, 10, 12, 14, 16).

Potassium 2,3,4-tris(dodecyloxy) benzenesulfonate (C12-K): As a typical synthesis procedure for the preparation of potassium 2,3,4-tris(alkyloxy) benzenesulfonates, herein the synthesis of C12-K is exemplified. 3,4,5-Trihydroxybenzenesulfonic acid (3.00 g, 14.5 mmol) and K_2CO_3 (20.41 g, 147.8 mmol) were mixed with 150 mL of dried DMF under nitrogen atmosphere. At 100 ℃, 14 mL (58.4 mmol) of 1-bromododecane were added dropwise. After stirring for 48 h at 100 ℃, the reaction mixture was subsequently slowly poured into 200 mL of ice water, and extracted with CH_2Cl_2 (3 × 100 mL). After removing the solvent via evaporation, the crude product was purified by column chromatography over silica gel with CH_3OH and CH_2Cl_2 (1/10, v/v). After recrystallization in CH_3OH, 2.30 g potassium 2,3,4-tris(dodecyloxy) benzenesulfonate as a white solid was obtained (yield 21%). ^{1}H NMR (400 MHz, $CDCl_3$) δ 7.10 (s, 2H), 3.96 (t, J = 6.5 Hz, 4H), 3.90 (t, J = 6.6 Hz, 2H), 1.82 – 1.57 (m, 6H), 1.49 –1.17 (m, 54H), 0.87 (t, J = 6.8 Hz, 9H). ESI-MS (*m/z*): $[M + K]^+$ calcd. for $C_{42}H_{77}KO_6S$, 748.51; found, 748.25.

Similarly, other potassium tris(alkyloxy) benzenesulfonates were obtained through the same synthetic protocol (Scheme S3). The characterization results are listed as below:

Potassium 2,3,4-tris(octyloxy) benzenesulfonate (C8-K): pale yellow waxy solid (yield 16%)**.** ^{1}H NMR (400 MHz, $CDCl_3$) δ 7.10 (s, 2H), 3.97 (t, J = 6.5 Hz, 4H), 3.91 (t, J = 6.6 Hz, 2H), 1.83 – 1.61 (m, 6H), 1.48 – 1.16 (m, 30H), 0.88 (t, J = 6.9 Hz, 9H).

ESI-MS (*m/z*): $[M + K]^+$ calcd. for $C_{30}H_{53}KO_6S$, 580.32; found, 580.61.

Potassium 2,3,4-tris(decyloxy) benzenesulfonate (C10-K): white waxy solid (yield 22%). ^1H NMR (400 MHz, $CDCl_3$) δ 7.10 (s, 2H), 3.97 (t, *J* = 6.5 Hz, 4H), 3.91 (t, *J* = 6.6 Hz, 2H), 1.83 – 1.62 (m, 6H), 1.45 – 1.19 (m, 42H), 0.88 (t, *J* = 6.9 Hz, 9H). ESI-MS (*m/z*): $[M + K]^+$ calcd. for $C_{36}H_{65}KO_6S$, 664.41; found, 664.80.

Potassium 2,3,4-tris(tetradecyloxy) benzenesulfonate (C14-K): white solid (yield 28%). ^1H NMR (400 MHz, $CDCl_3$) δ 7.12 (s, 2H), 3.96 (t, *J* = 6.4 Hz, 4H), 3.91 (t, *J* = 6.6 Hz, 2H), 1.80 – 1.61 (m, 6H), 1.50 – 1.17 (m, 66H), 0.88 (t, *J* = 6.8 Hz, 9H). ESI-MS (*m/z*): $[M + K]^+$ calcd. for $C_{48}H_{89}KO_6S$, 832.60; found, 833.12.

Potassium 2,3,4-tris(hexadecyloxy) benzenesulfonate (C16-K): white solid (yield 39%). ^1H NMR (400 MHz, $CDCl_3$) δ 7.12 (s, 2H), 3.97 (t, *J* = 6.5 Hz, 4H), 3.91 (t, *J* = 6.6 Hz, 2H), 1.86 – 1.57 (m, 6H), 1.48 – 1.17 (m, 78H), 0.88 (t, *J* = 6.8 Hz, 9H). ESI-MS (*m/z*): $[M + K]^+$ calcd. for $C_{54}H_{101}KO_6S$, 916.70; found, 916.21.

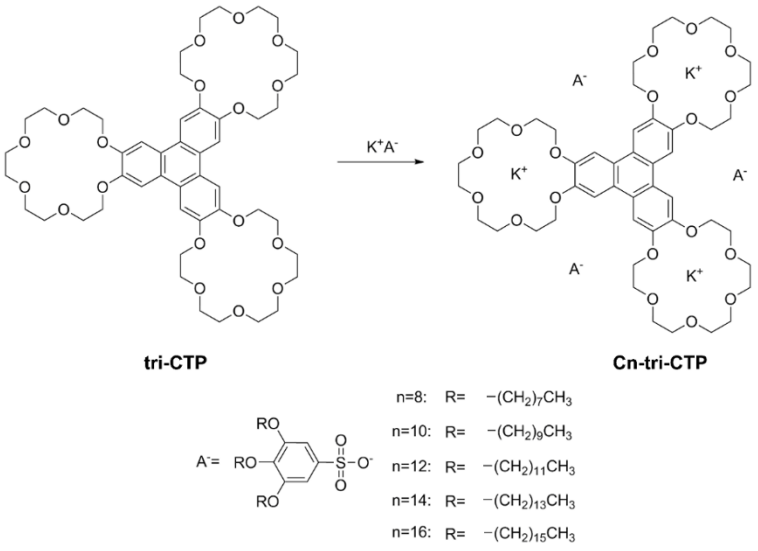

Scheme S4 Schematic representation of the ILC complexes from tris(18-crown-6)triphenylene (**tri-CTP**) and various potassium sulfonates **Cn-K** (n = 8, 10, 12, 14, 16) of variant length alkyl tails through host-guest complexation between macrocyclic crown ether and K^+.

The host-guest complexes were prepared according to the similar procedure as presented in our previous report[1] with a little modification (Scheme S4).

Tris(18-crown-6)triphenylene **tri-CTP** and corresponding potassium salts K^+A^- (**Cn-K**, 4 eq) were dissolved in 2 mL CH_2Cl_2. After continuously stirring for 24~48 h at room temperature until the solvent was totally evaporated, the obtained primitive complex samples were dissolved with small amount of methanol and precipitated in water to remove the residual excess potassium salts. After repeating the dissolution/precipitation purification procedure for several times, then dried to constant weight under vacuum, the final complex products were obtained.

C8-tri-CTP: pale yellow waxy solid (yield 85%). ^{1}H NMR (400 MHz, $CDCl_3$) δ 7.78 (s, 6H), 7.05 (s, 6H), 4.39 – 4.33 (m, 12H), 4.03 – 3.98 (m, 12H), 3.92 (t, *J* = 6.5 Hz, 12H), 3.86 (t, *J* = 6.6 Hz, 6H), 3.77 (dd, *J* = 5.8, 2.7 Hz, 12H), 3.69 (dd, *J* = 5.8, 2.5 Hz, 12H), 3.65 (s, 12H), 1.80 – 1.56 (m, 18H), 1.44 – 1.10 (m, 90H), 0.83 (t, *J* = 6.8 Hz, 27H). ^{13}C NMR (100 MHz, $CDCl_3$) δ 152.55, 148.59, 141.38, 139.88, 123.66, 106.99, 104.45, 73.34, 70.66, 70.58, 69.92 – 68.61 (m), 31.61, 29.91 – 28.76 (m), 26.16, 22.65, 14.03.

C10-tri-CTP: pale yellow waxy solid (yield 87%). ^{1}H NMR (400 MHz, $CDCl_3$) δ 7.80 (s, 6H), 7.06 (s, 6H), 4.40 – 4.34 (m, 12H), 4.05 – 4.00 (m, 12H), 3.92 (t, *J* = 6.5 Hz, 12H), 3.87 (t, *J* = 6.6 Hz, 6H), 3.79 (dd, *J* = 5.7, 2.9 Hz, 12H), 3.72 (dd, *J* = 5.7, 2.8 Hz, 12H), 3.67 (s, 12H), 1.77 – 1.60 (m, 18H), 1.43 – 1.15 (m, 126H), 0.85 (t, *J* = 6.9 Hz, 27H). ^{13}C NMR (100 MHz, $CDCl_3$) δ 152.56, 148.61, 141.34, 139.22, 123.69, 107.07, 104.46, 73.35, 70.67, 70.61, 69.97 – 68.62 (m), 31.82, 29.98 – 28.91 (m), 26.18, 22.70, 14.09.

C12-tri-CTP: white solid (yield 92%). ^{1}H NMR (400 MHz, $CDCl_3$) δ 7.83 (s, 6H), 7.11 (s, 6H), 4.42 – 4.36 (m, 12H), 4.07 – 4.02 (m, 12H), 3.95 (t, *J* = 6.5 Hz, 12H), 3.91 (t, *J* = 6.6 Hz, 6H), 3.82 (dd, *J* = 5.7, 2.9 Hz, 12H), 3.74 (dd, *J* = 5.7, 2.8 Hz, 12H), 3.69 (s, 12H), 1.82 – 1.62 (m, 18H), 1.50 – 1.16 (m, 162H), 0.87 (t, *J* = 6.8 Hz, 27H). ^{13}C NMR (100 MHz, $CDCl_3$) δ 152.61, 148.70, 140.71, 139.20, 123.78, 107.32, 104.51, 73.36, 70.78, 70.69, 69.70 – 69.07 (m), 31.93, 30.32 – 29.21 (m), 26.19, 22.73, 14.13.

C14-tri-CTP: white solid (yield 90%). ^{1}H NMR (400 MHz, $CDCl_3$) δ 7.83 (s, 6H),

7.10 (s, 6H), 4.42 – 4.36 (m, 12H), 4.07 – 4.02 (m, 12H), 3.94 (t, *J* = 6.4 Hz, 12H), 3.90 (t, *J* = 6.6 Hz, 6H), 3.83 (dd, *J* = 5.7, 2.8 Hz, 12H), 3.74 (dd, *J* = 5.7, 2.5 Hz, 12H), 3.69 (s, 12H), 1.79 – 1.62 (m, 18H), 1.49 – 1.14 (m, 198H), 0.87 (t, *J* = 6.7 Hz, 27H). ^{13}C NMR (100 MHz, $CDCl_3$) δ 152.58, 148.65, 141.24, 138.95, 123.73, 107.20, 104.48, 73.35, 70.73, 70.65, 69.96 – 68.07 (m), 31.92, 30.55 – 28.45 (m), 26.20, 22.73, 14.12.

C16-tri-CTP: white solid (yield 93%). ^{1}H NMR (400 MHz, $CDCl_3$) δ 7.83 (s, 6H), 7.12 (s, 6H), 4.41 – 4.36 (m, 12H), 4.07 – 4.02 (m, 12H), 3.96 (t, *J* = 6.5 Hz, 12H), 3.90 (t, *J* = 6.6 Hz, 6H), 3.82 (dd, *J* = 5.9, 2.9 Hz, 12H), 3.74 (dd, *J* = 5.9, 2.8 Hz, 12H), 3.69 (s, 12H), 1.79 – 1.62 (m, 18H), 1.46 – 1.19 (m, 234H), 0.87 (t, *J* = 6.8 Hz, 27H). ^{13}C NMR (101 MHz, $CDCl_3$) δ 152.59, 148.68, 141.17, 138.98, 123.75, 107.27, 104.49, 73.35, 70.75, 70.66, 70.10 – 68.61 (m), 31.93, 30.81 – 27.92 (m), 26.20, 22.73, 14.12.

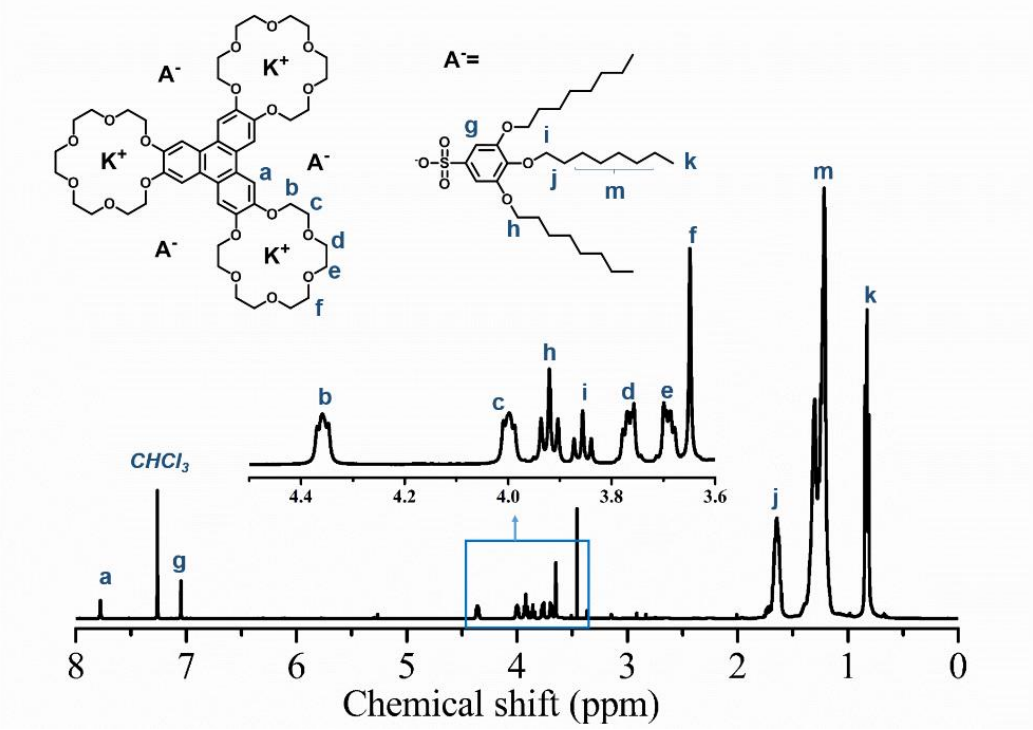

Fig. S2 ^{1}H NMR spectrum of the complex C8-tri-CTP in $CDCl_3$.

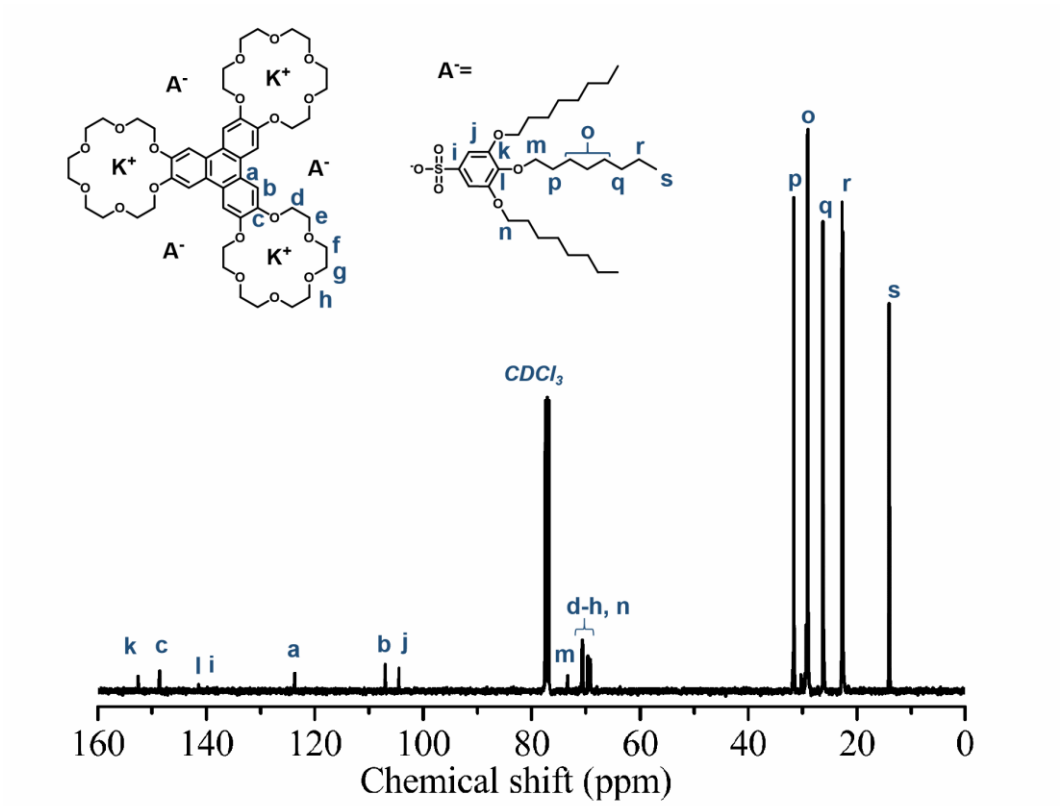

Fig. S3 ^{13}C NMR spectrum of the complex C8-tri-CTP in $CDCl_3$.

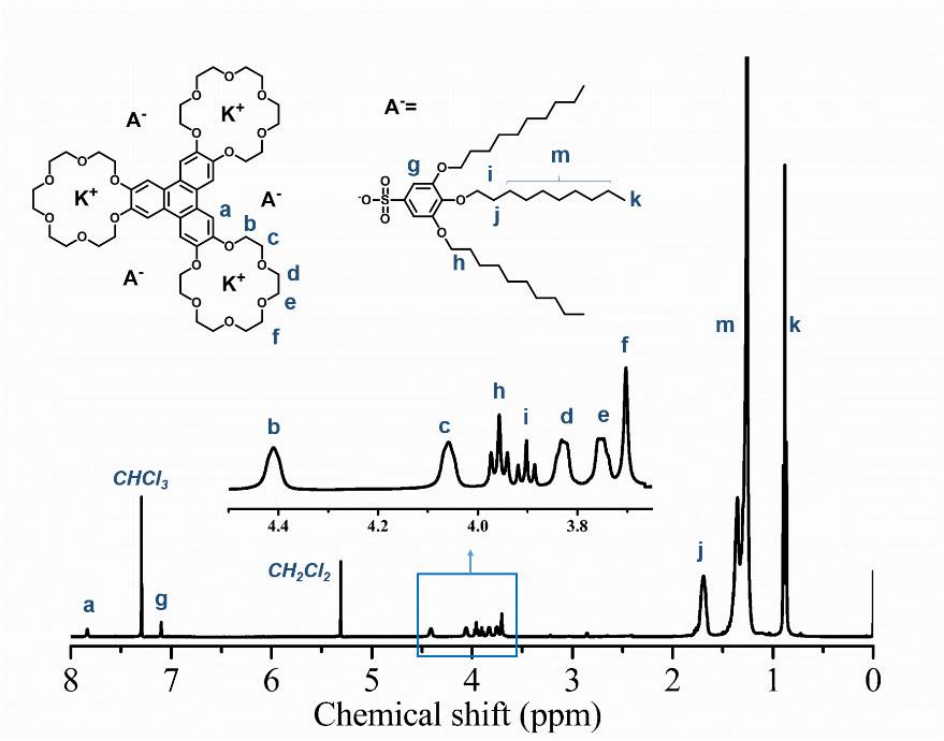

Fig. S4 ^{1}H NMR spectrum of the complex C10-tri-CTP in $CDCl_3$.

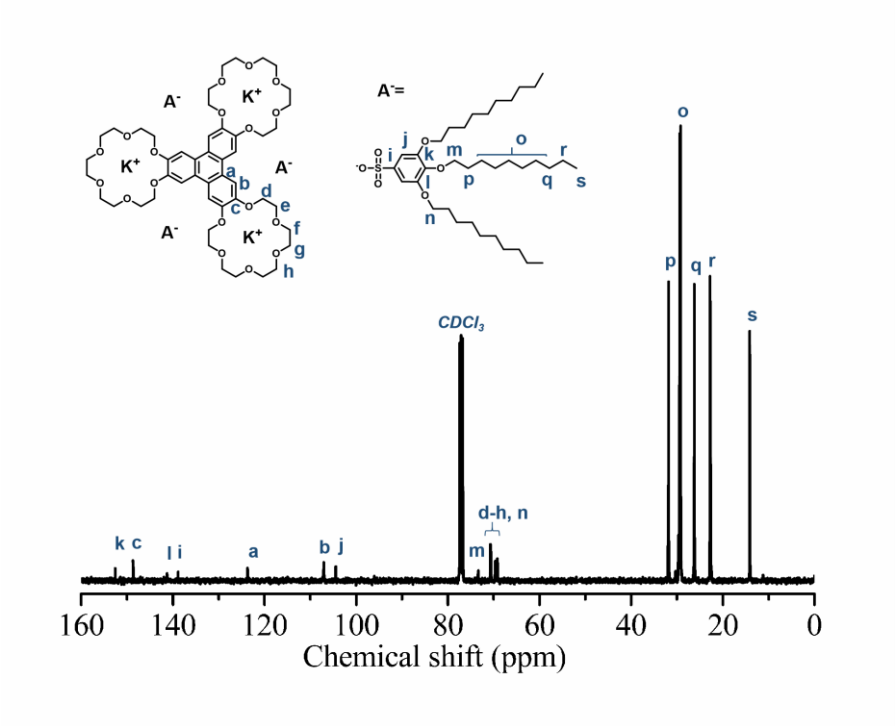

Fig. S5 ^{13}C NMR spectrum of the complex C10-tri-CTP in $CDCl_3$.

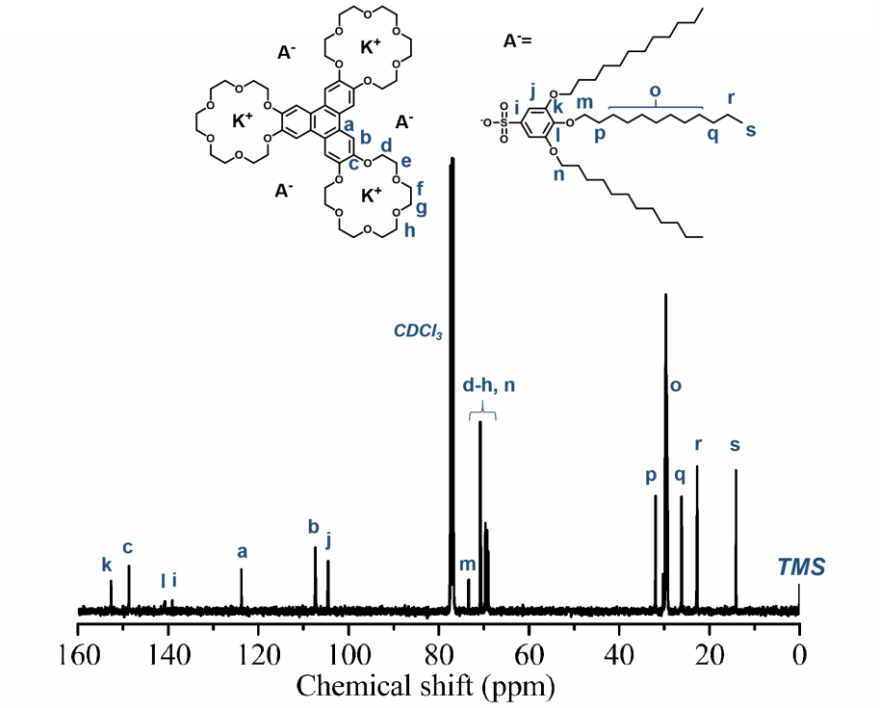

Fig. S6 ^{13}C NMR spectrum of the complex C12-tri-CTP in $CDCl_3$.

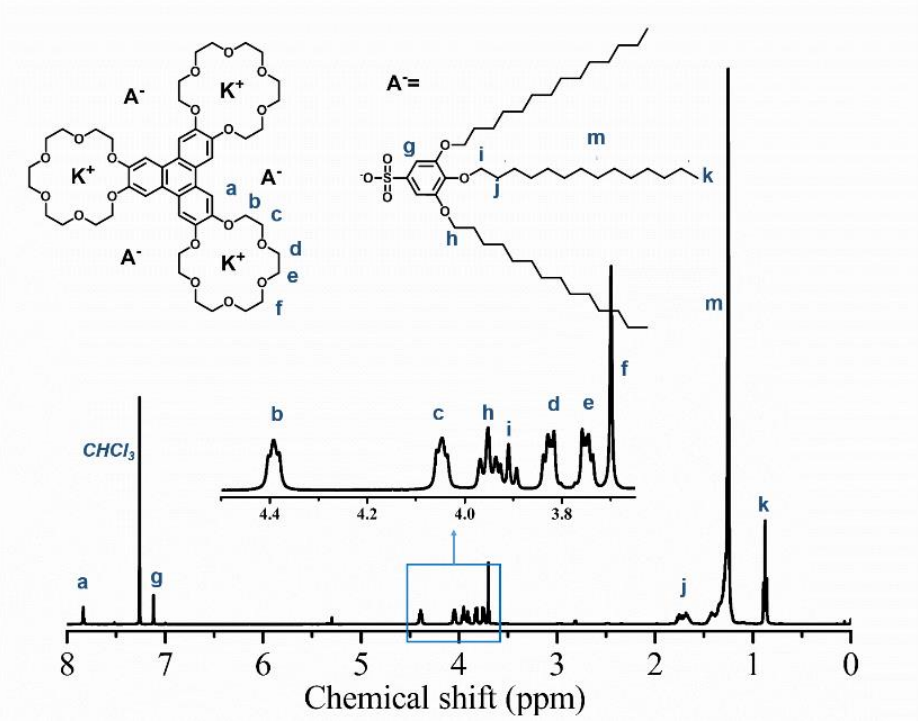

Fig. S7 ^{1}H NMR spectrum of the complex C14-tri-CTP in $CDCl_3$.

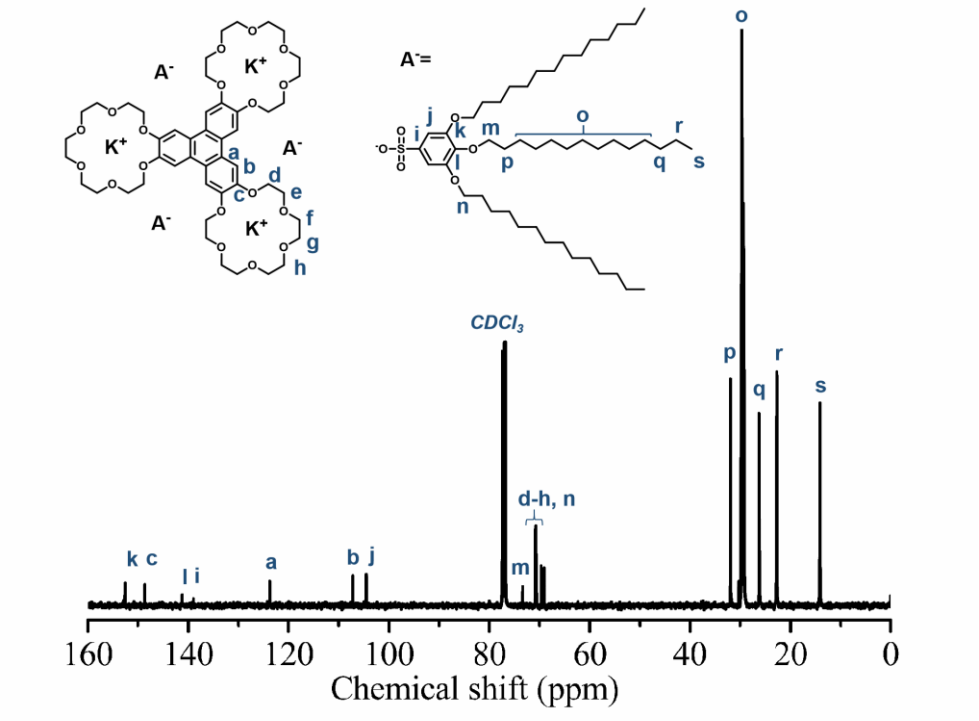

Fig. S8 ^{13}C NMR spectrum of the complex C14-tri-CTP in $CDCl_3$.

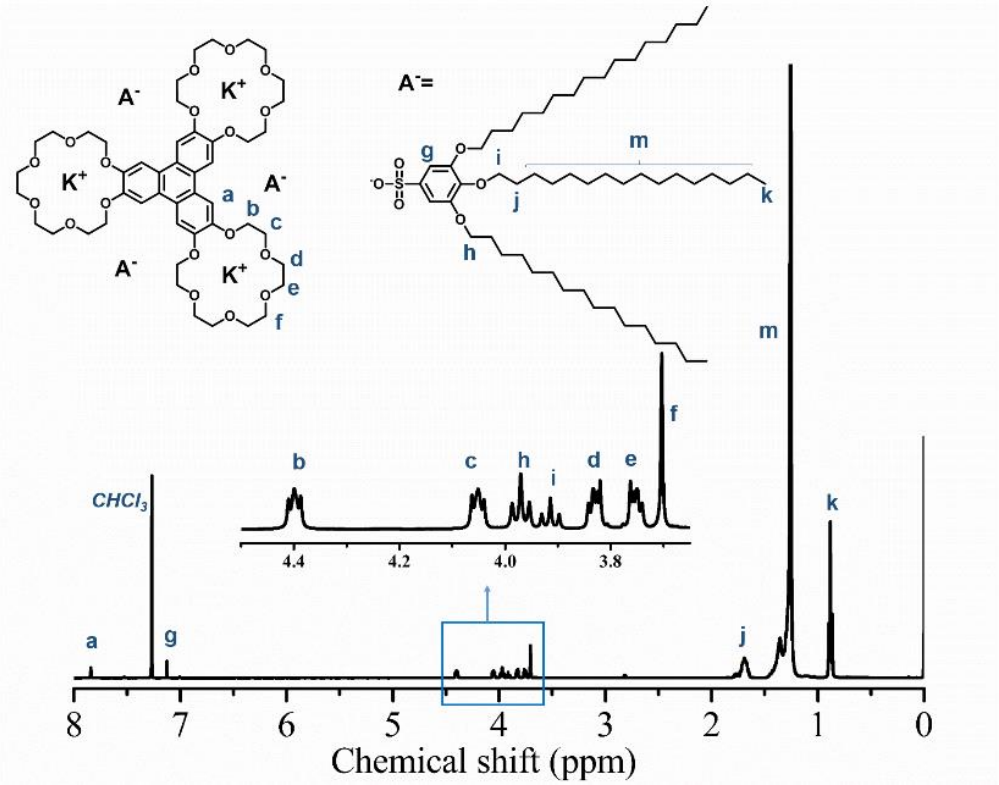

Fig. S9 ^{1}H NMR spectrum of the complex C16-tri-CTP in $CDCl_3$.

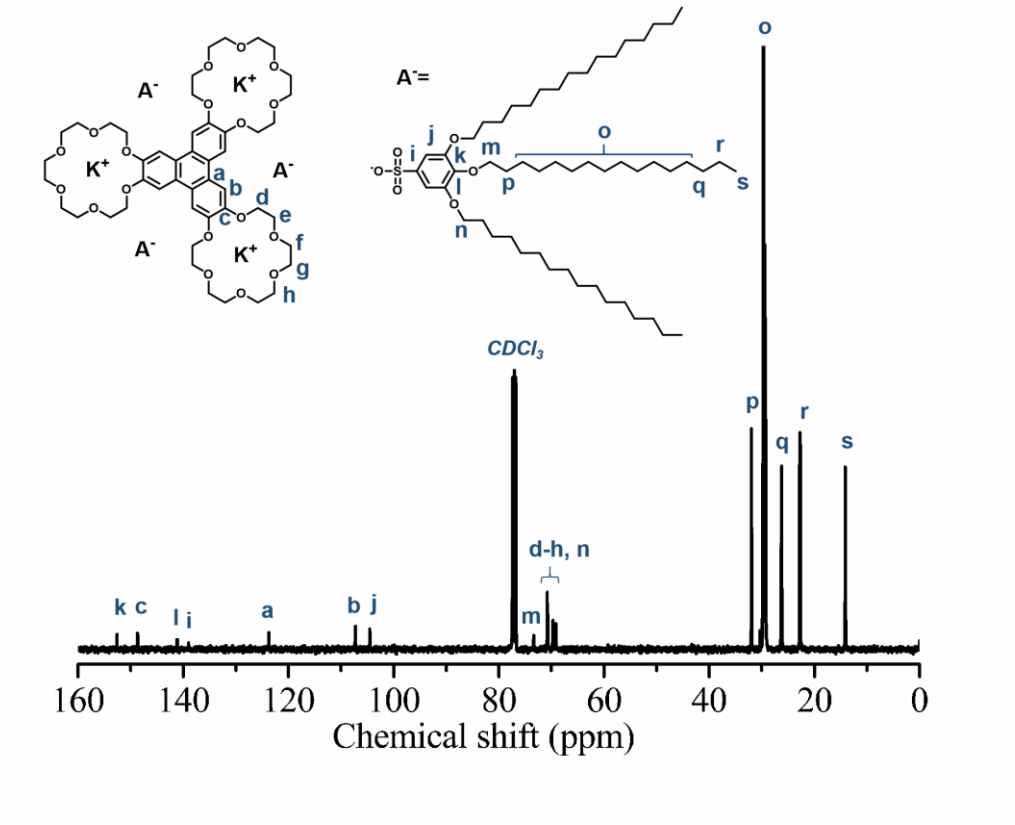

Fig. S10 ^{13}C NMR spectrum of the complex C16-tri-CTP in $CDCl_3$.

2. Other supplementary figures and tables

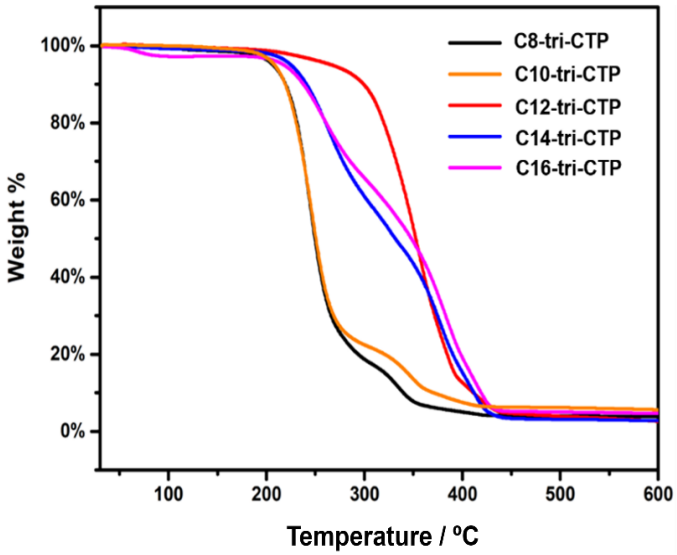

Compound	$T_{5\%}$(°C)
C8-tri-CTP	207
C10-tri-CTP	208
C12-tri-CTP	267
C14-tri-CTP	225
C16-tri-CTP	218

Fig. S11 Thermal gravimetric analysis (TGA) curves of the series of complexes at a heating rate of 20 ℃ min^{-1} under nitrogen atmosphere, with the temperatures of 5% weight loss ($T_{5\%}$) listed.

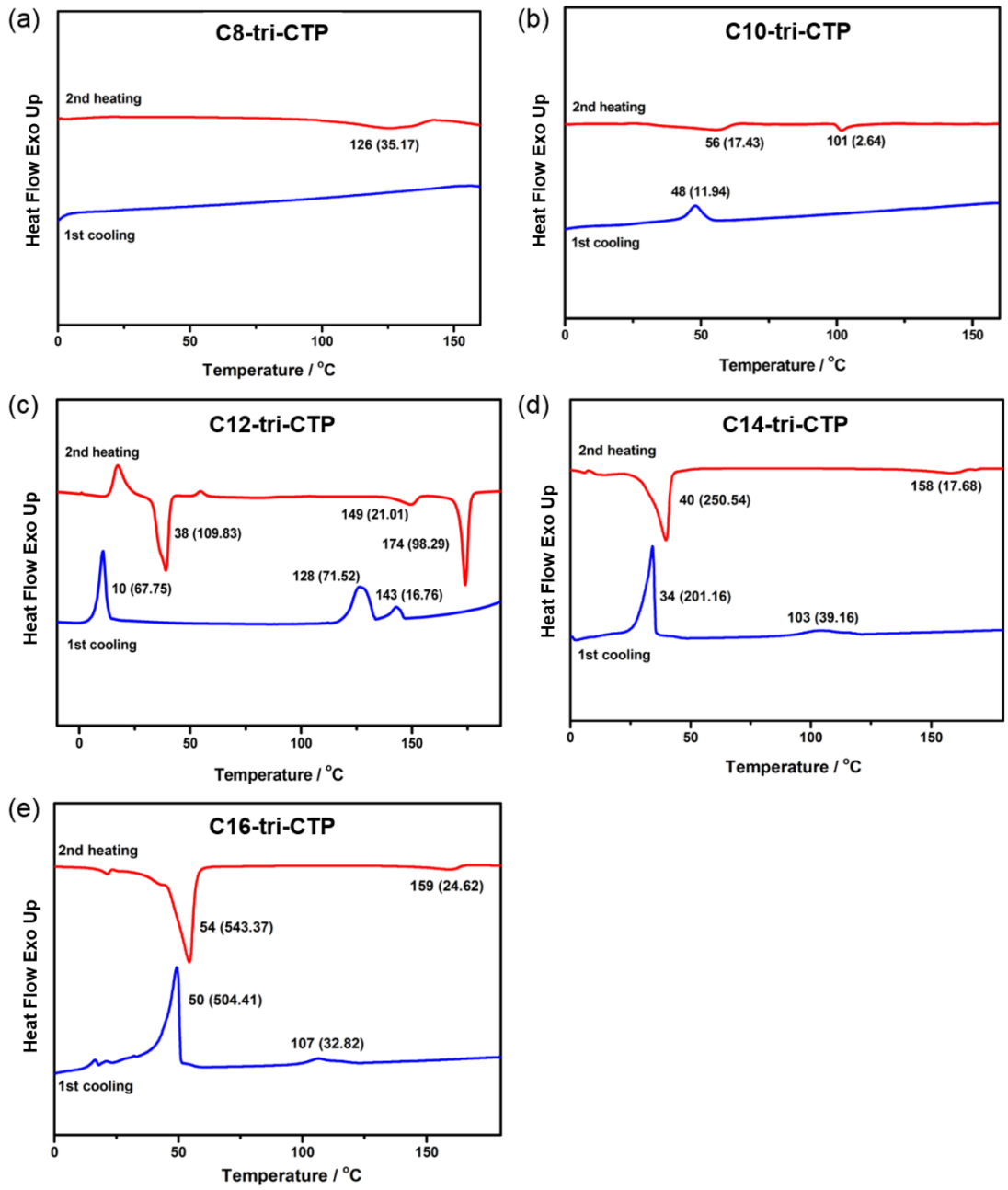

Fig. S12 DSC traces of the series of complexes (a) C8-tri-CTP, (b) C10-tri-CTP, (c) C12-tri-CTP, (d) C14-tri-CTP, and (e) C16-tri-CTP at a heating/cooling rate of 10 ℃/min, indicating with transition peak temperatures (in ℃) and associated enthalpy changes (in parentheses, in J g^{-1}).

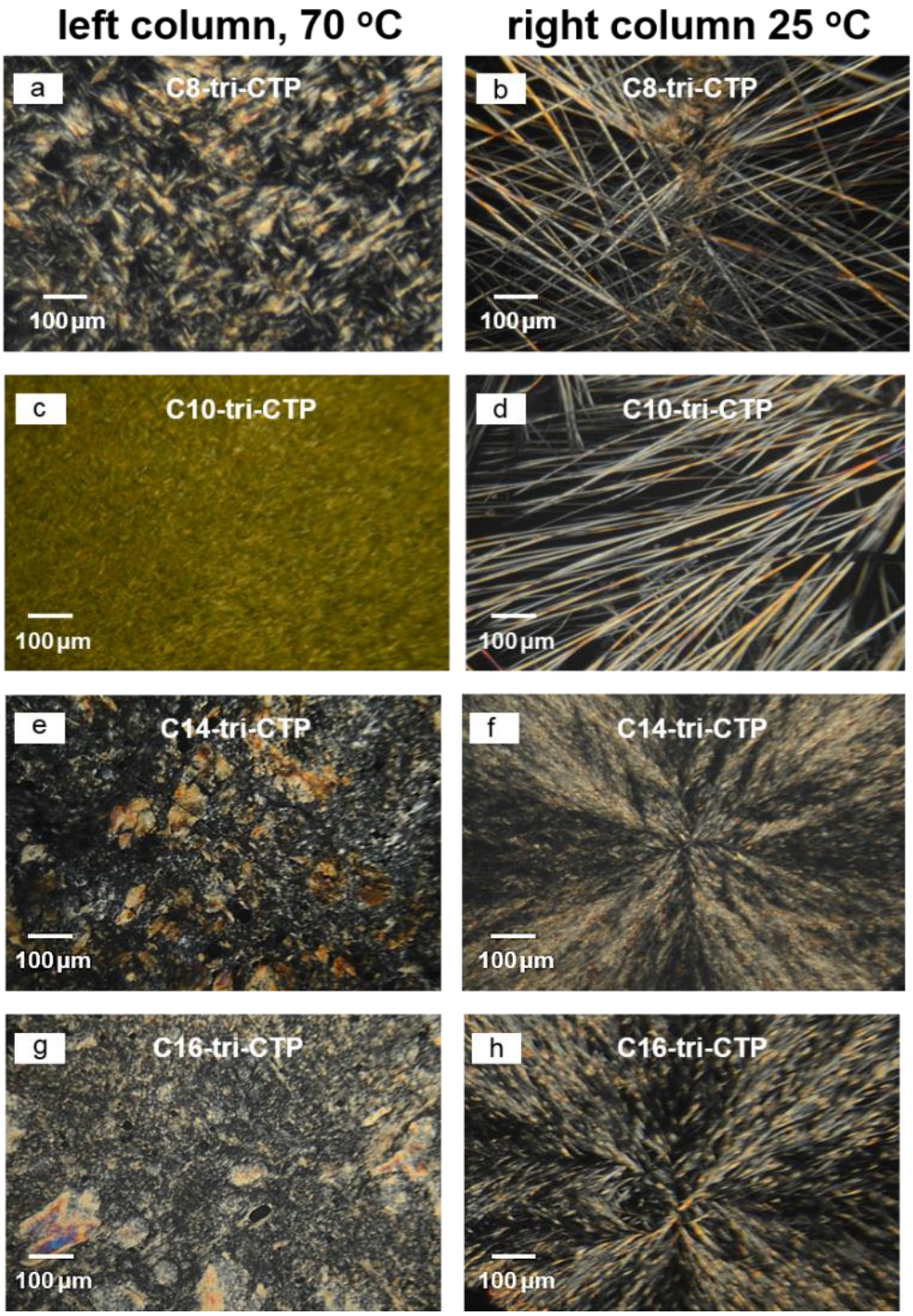

Fig. S13 Representative POM images under crossed polarizers of the series complexes at room temperature or the selected temperatures after slowly cooling from the isotropic state:
(a) C8-tri-CTP, 70 ℃; (b) C8-tri-CTP, 25 ℃; (c) C10-tri-CTP, 70 ℃; (d) C10-tri-CTP, 25 ℃;
(e) C14-tri-CTP, 70 ℃; (f) C14-tri-CTP, 25 ℃; (g) C16-tri-CTP, 70 ℃; (h) C16-tri-CTP, 25 ℃.

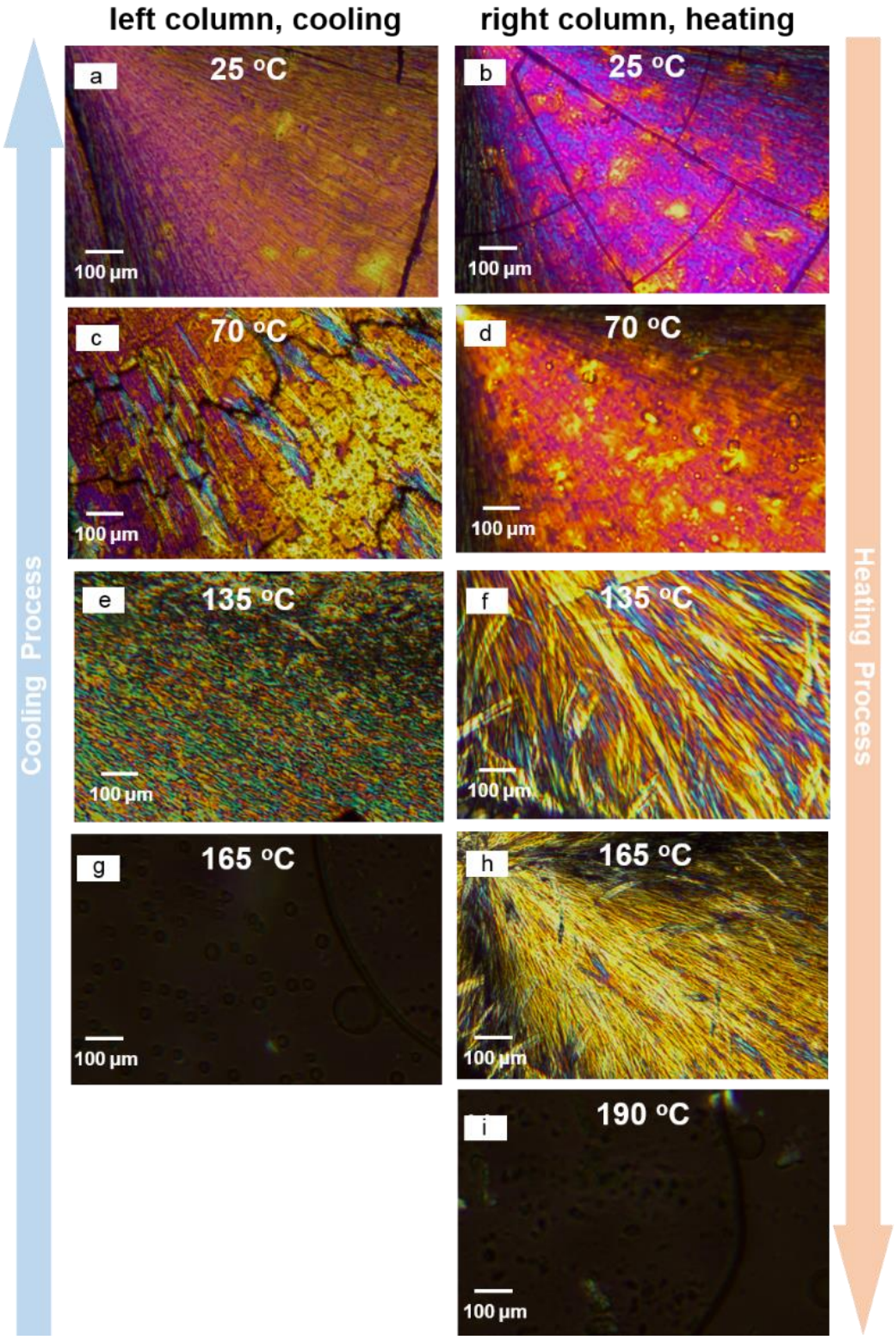

Fig. S14 Representative POM images under the crossed polarizers of the complex C12-tri-CTP at (a) 25 ℃, (c) 70 ℃, (e) 135 ℃, (g) 165 ℃ upon slowly cooling from the isotropic state (left column), and at (b) 25 ℃, (d) 70 ℃, (f) 135 ℃, (h) 165 ℃ (i) 190 ℃ upon heating the annealed sample from room temperature (right column).

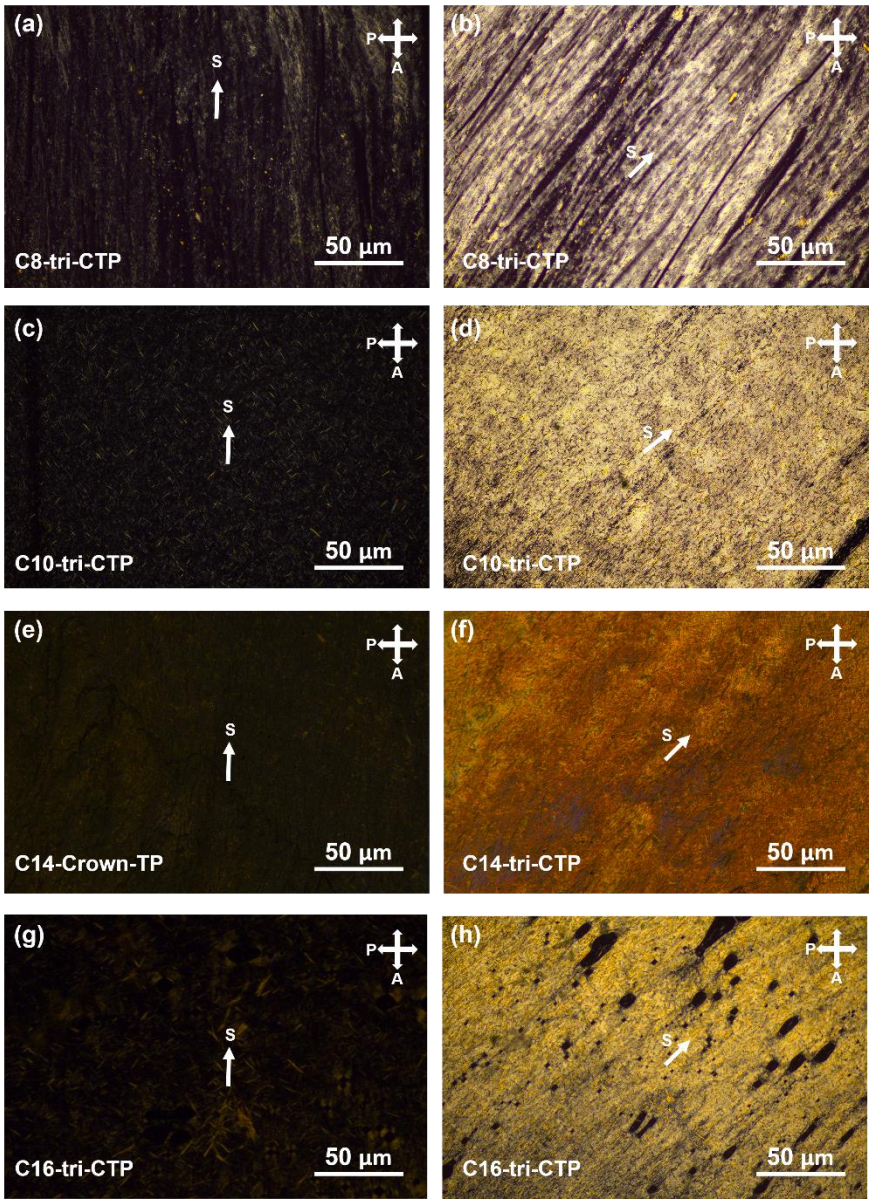

Fig. S15 Representative POM images of the series complexes of Cn-tri-CTP (*n* = 8, 10, 14, 16) after shearing at 70 ℃. The shearing direction is in parallel (a, c, e, g) or tilting 45 °(b, d, f, h) to the analyzer. Rotating the shear-aligned sample every 45 °producing dark (a, c, e, g) or bright (b, d, f, h) images under cross-polarizers periodically. The directions of shearing (S), polarizer (P) and analyzer (A). (a, b) C8-tri-CTP; (c, d) C10-tri-CTP; (e, f) C14-tri-CTP; (g, h) C16-tri-CTP.

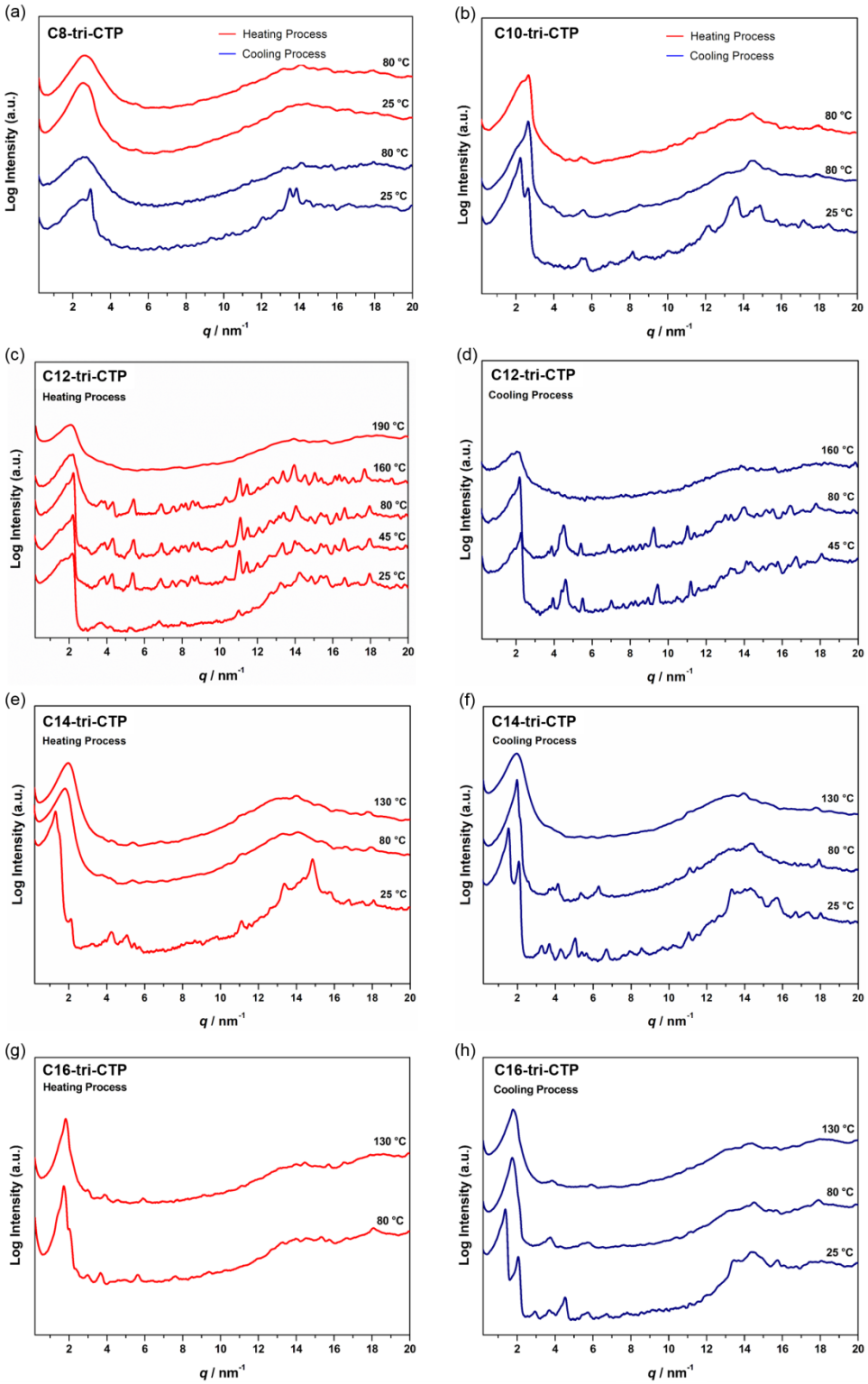

Fig. S16 Variable temperature SAXS/WAXS analyses of the series of complexes during cooling and/or upon heating: (a) C8-tri-CTP; (b) C10-tri-CTP; (c, d) C12-tri-CTP; (e, f) C14-tri-CTP; (g, h) C16-tri-CTP. For all investigations, with the red line standing for the heating process, and the blue line for the cooling process, with the temperatures labelled on the corresponding curves.

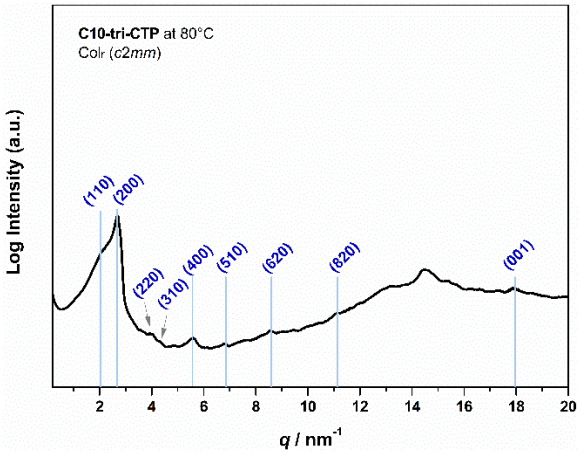

Fig. S17 SAXS/WAXS pattern with proposed indices of the ionic complex C10-tri-CTP exhibiting center-faced rectangular columnar LC mesophase Col_r (*c*2*mm*) at 80 ℃.

Table S1 SAXS/WAXS data and structural analyses of C10-tri-CTP

	hkl	q_{obs} (nm^{-1})	d_{obs} (nm)	d_{calc} (nm)	Intensity[a] ($I\ q^2$)	Multiplicity	Phase[b]
	110	1.97	3.19	3.19	35	4	0
	200	2.67	2.35	2.35	100	2	0
C10-tri-CTP	220	3.97	1.58	1.60	1.1	4	0
80 ℃	310	4.30	1.46	1.47	1.5	4	π
Col_r (*c*2*mm*)	400	5.46	1.15	1.17	7.1	2	0
a = 4.70 nm	510	6.80	0.92	0.92	1.7	4	/
b = 4.35 nm	620	8.56	0.73	0.74	1.6	4	/
P^c = 1.36 g cm^{-3}	820	11.12	0.56	0.57	2.1	4	/
	001(π-stacking)	17.92	0.35	/	/	/	/

[a] The peak intensities were calculated after Lorentz and multiplicity corrections. [b] Only the first 5 orders were used to reconstruct the electron density map. [c] The calculated density ρ based on measured lattice parameters was determined as $\rho = MZ/(N_A \cdot V_{unit\ cell})$, $V_{unit\ cell}(Col_r) = a\ b\ c$, a = 4.70 nm, b = 4.35 nm, c = 3.5 Å and M is the molecular weight of C10-tri-CTP of 2926 g mol^{-1}. Based on these lattice parameters, only a unit cell containing two groups of C10-tri-CTP complex (Z = 2) gives a reasonable density.

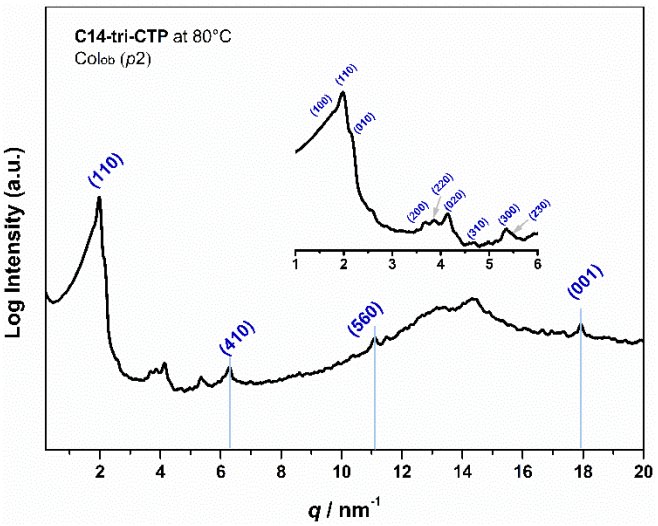

Fig. S18 SAXS/WAXS pattern with proposed indices of the ionic complex C14-tri-CTP exhibiting oblique columnar LC mesophase Col_{ob} (*p*2) at 80 ℃.

Table S2 SAXS/WAXS data and structural analyses of C14-tri-CTP

	hkl	q_{obs} (nm^{-1})	d_{obs} (nm)	d_{calc} (nm)	Intensity[a] ($I\,q^2$)	Multiplicity	Phase[b]
	100	1.80	3.53	3.53	67	2	0
	110	1.95	3.23	3.23	100	2	0
C14-tri-CTP	010	2.07	3.03	3.03	39	2	π
80 ℃	200	3.64	1.73	1.76	3.0	2	π
Col_{ob} (*p*2)	220	3.87	1.62	1.62	6.1	2	π
a = 4.03 nm	020	4.14	1.52	1.51	9.2	2	π
b = 3.50 nm	310	4.67	1.34	1.35	0.8	2	π
θ = 60.0 °	300	5.33	1.18	1.18	2.1	2	/
ρ^c = 1.33 g cm^{-3}	230	5.46	1.15	1.16	1.8	2	/
	410	6.28	1.00	0.99	4.1	2	/
	560	11.07	0.57	0.57	6.3	2	/
	001(π-stacking)	17.92	0.35	/	/	/	/

[a] The peak intensities were calculated after Lorentz and multiplicity corrections. [b] Only the first 7 orders were used to reconstruct the electron density map. [c] The calculated density ρ based on measured lattice parameters was determined as $\rho = M Z/(N_A \cdot V_{unit\ cell})$, $V_{unit\ cell}(Col_{ob}) = a \cdot b \cdot sin\theta \cdot c$, *a* = 4.03 nm, *b* = 3.50 nm, *c* = 3.5 Å, θ = 60 °and *M* is the molecular weight of C14-tri-CTP of 3431 g mol^{-1}. Based on these lattice parameters, only a unit cell containing only one group of C14-tri-CTP complex (*Z* = 1) gives a reasonable density.

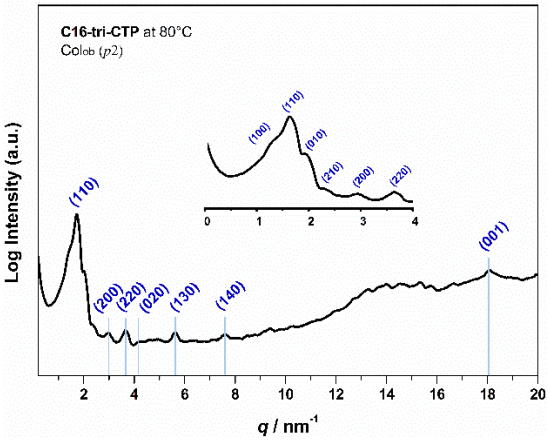

Fig. S19 SAXS/WAXS pattern with proposed indices of the ionic complex C16-tri-CTP exhibiting oblique columnar LC mesophase Col_{ob} (*p*2) at 80 ℃.

Table S3 SAXS/WAXS data and structural analyses of C16-tri-CTP

	hkl	q (nm^{-1})	d_{obs} (nm)	d_{calc} (nm)	Intensity[a] ($I\,q^2$)	Multiplicity	Phase[b]
	100	1.44	4.36	4.36	82	2	0
C16-tri-CTP	110	1.76	3.57	3.57	100	2	0
80 ℃	010	2.07	3.03	3.02	62	2	π
Col_{ob} (*p*2)	210	2.40	2.62	2.56	4.5	2	π
a = 5.23 nm	200	2.93	2.14	2.18	14	2	π
b = 3.62 nm	220	3.58	1.75	1.78	21	2	π
θ = 56.5 °	020	4.16	1.51	1.51	5.4	2	π
ρ^c = 1.11 g cm^{-3}	130	5.60	1.12	1.13	16	2	/
	140	7.61	0.83	0.82	10	2	/
	001(π-stacking)	18.10	0.35	/	/	/	/

[a] The peak intensities were calculated after Lorentz and multiplicity corrections. [b] Only the first 7 orders were used to reconstruct the electron density map. [c] The calculated density ρ based on measured lattice parameters was determined as $\rho = M Z/(N_A \cdot V_{unit\ cell})$, $V_{unit\ cell}(Col_{ob}) = a \cdot b \cdot \sin\theta \cdot c$, a = 5.23 nm, b = 3.62 nm, c = 3.5 Å, θ = 56.5 ° and M is the molecular weight of C16-tri-CTP of 3684 g·mol^{-1}. Based on these lattice parameters, only a unit cell containing only one group of C16-tri-CTP complex (Z = 1) gives a reasonable density.

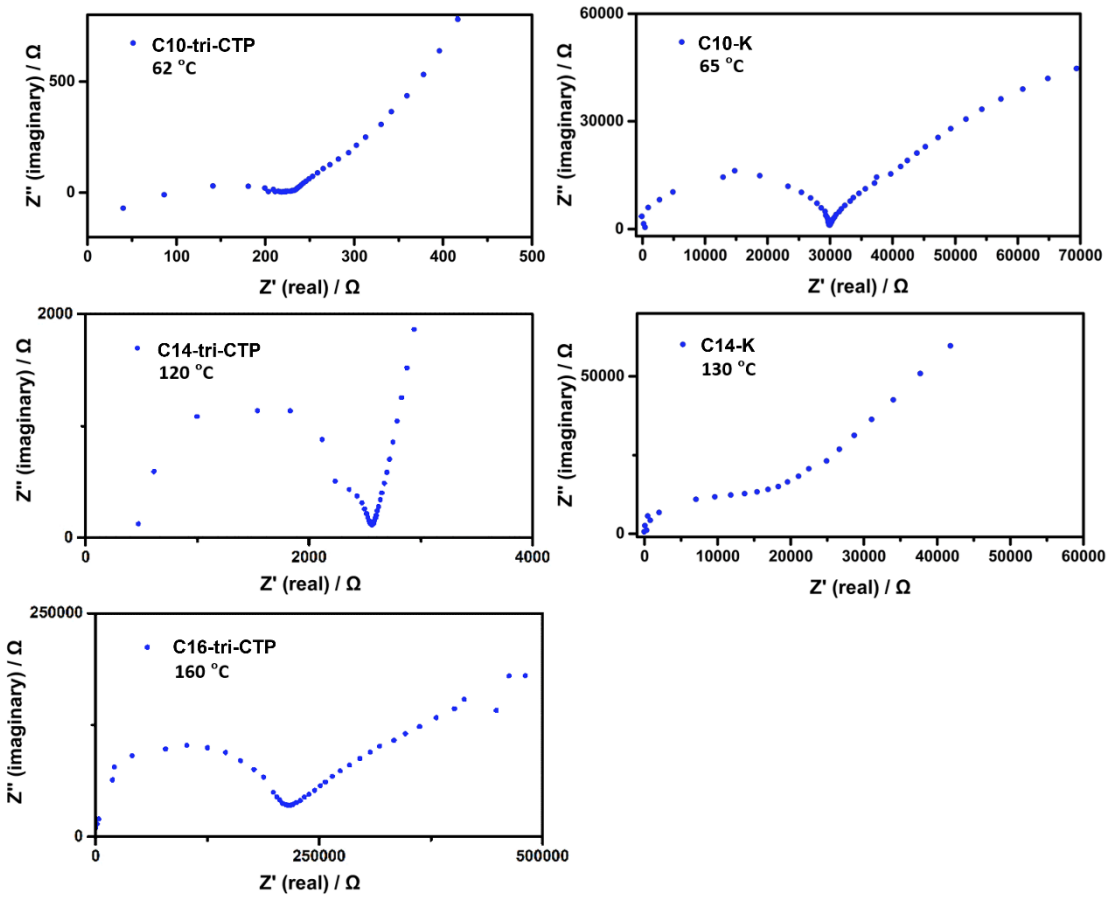

Fig. S20 Representative electrochemical AC impedance curves of the C10-tri-CTP, C10-K, C14-tri-CTP, C14-K and C16-tri-CTP, as tested at the indicated temperatures.

Table S4 Variable temperature ionic conductivities of the series complexes (C10-tri-CTP, C14-tri-CTP, C16-tri-CTP) and the comparative guest compounds (C10-K, C14-K) in their unoriented state.

C10-tri-CTP		**C10-K**		**C14-tri-CTP**		**C14-K**		**C16-tri-CTP**	
T / ℃	**σ** / S cm^{-1}	**T** / ℃	**σ** / S cm^{-1}	**T** / ℃	**σ** / S cm^{-1}	**T** / ℃	**σ** / S cm^{-1}	**T** / ℃	**σ** / S cm^{-1}
		25	2.01E-06						
30	1.33E-03	30	2.28E-06						
33	1.43E-03	35	3.33E-06						
36	1.74E-03	40	7.37E-06						
41	2.44E-03	45	1.19E-05	45	1.39E-04				
45	2.90E-03	50	1.63E-05	55	3.00E-04				
50	3.65E-03	55	2.17E-05	60	4.02E-04				
55	4.30E-03	60	2.92E-05	65	5.05E-04				
60	4.63E-03	65	3.99E-05	70	6.09E-04				
62	5.42E-03	70	5.31E-05	75	6.93E-04				
68	6.47E-03	75	6.96E-05	80	7.27E-04				
70	6.94E-03	80	8.69E-05	85	8.35E-04				
72	7.68E-03	85	1.10E-04	90	9.08E-04				
75	8.17E-03	90	1.26E-04	95	1.07E-03				
77	8.30E-03	95	1.42E-04	100	1.19E-03				
80	9.60E-03	100	1.63E-04	105	1.31E-03	103	3.50E-06		
83	1.01E-02	105	1.83E-04	110	1.49E-03	108	7.48E-06		
90	1.24E-02	110	1.97E-04	115	1.72E-03	115	1.57E-05		
93	1.29E-02			120	1.86E-03	124	2.64E-05	120	3.18E-07
97	1.36E-02			125	2.03E-03	130	4.39E-05	140	1.56E-06
100	1.48E-02			130	2.08E-03	137	7.26E-05	150	3.77E-06
102	1.55E-02			135	2.38E-03			160	5.61E-06
105	1.58E-02			140	2.66E-03			170	6.92E-06
107	1.65E-02			145	2.91E-03			180	8.38E-06
				150	3.12E-03			190	1.03E-05
				155	3.17E-03				
				160	3.55E-03				

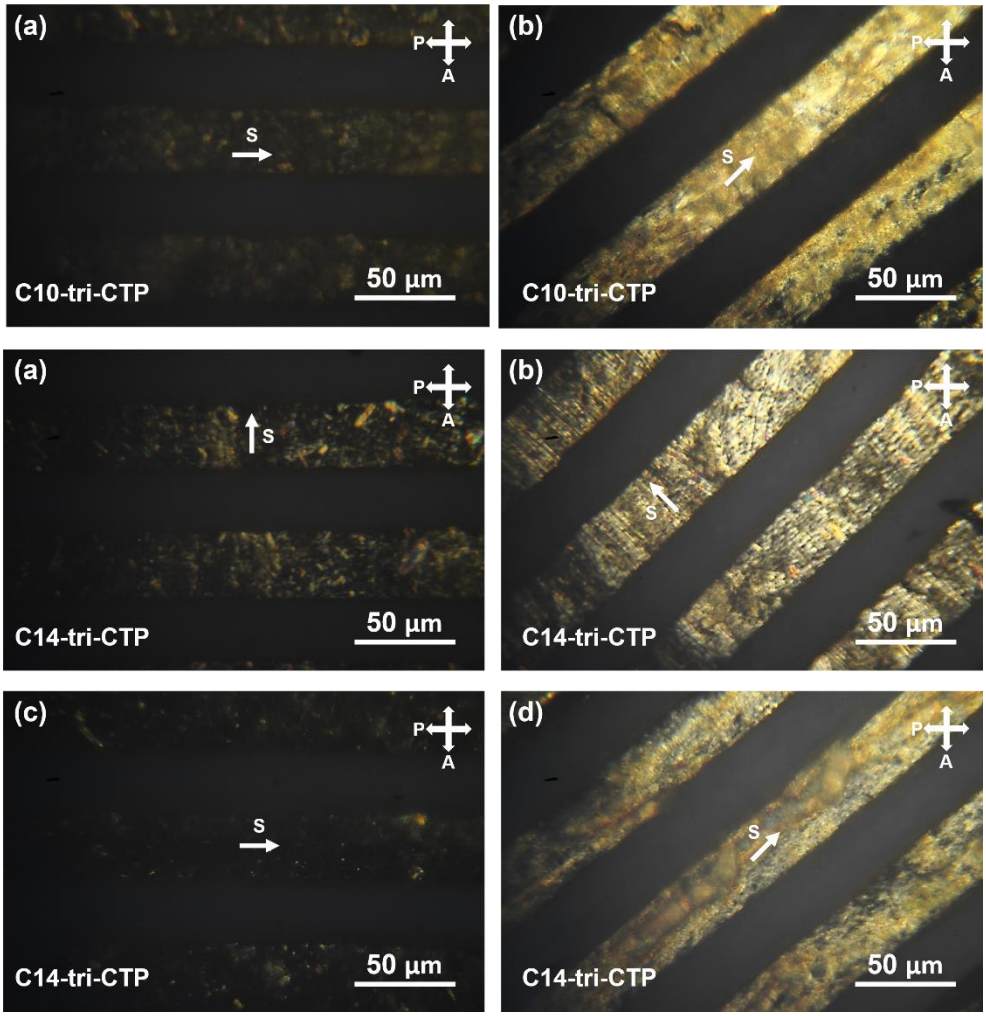

Fig. S21 Polarized optical micrographs of C10-tri-CTP (a, b) and C14-tri-CTP (c, d, e, f) with uniaxial orientation of the columns in the LC mesophase state (65 ℃) on the interdigital electrodes. The shearing direction was parallel (a, b, e, f) or perpendicular (c, d) to the electrodes. Rotating the sample every 45 ° produced dark (a, c, e) or bright (b, d, f) images under crossed polarizers periodically, indicated with white arrows of shearing direction (S), polarizer (P) and analyzer (A) axes.

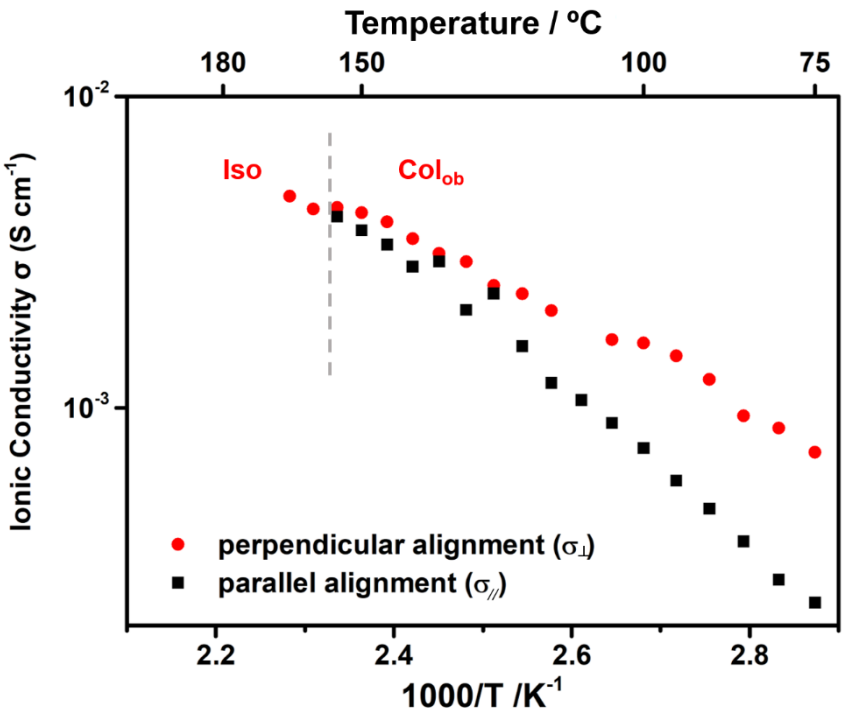

Fig. S22 Ionic conductivities of C14-tri-CTP with uniaxial orientation of the columns aligned parallel ($\sigma_{//}$) and perpendicular ($\sigma_{\perp}$) to the interdigital electrodes by macroscopically shearing. The heating rate is 5 ℃/min.

Table S5 Variable temperature ionic conductivities of C10-tri-CTP and C14-tri-CTP thin films in uniaxial orientation with the columns in the columnar state aligned parallel ($\sigma_{/\!/}$) or perpendicular ($\sigma_{\perp}$) to the interdigital electrodes through shearing.

C10-tri-CTP				**C14-tri-CTP**			
Perpendicular		**Parallel**		**Perpendicular**		**Parallel**	
T / ℃	**σ** / S cm^{-1}	**T** / ℃	**σ** / S cm^{-1}	**T** / ℃	**σ** / S cm^{-1}	**T** / ℃	**σ** / S cm^{-1}
40	2.60E-03	40	3.20E-04	40	2.09E-04	50	3.09E-05
42	3.32E-03	45	4.44E-04	45	2.12E-04	55	4.58E-05
47	4.35E-03	50	5.55E-04	50	2.70E-04	60	7.21E-05
50	6.88E-03	55	6.01E-04	55	3.04E-04	65	1.02E-04
55	8.85E-03	60	8.27E-04	60	3.52E-04	70	1.55E-04
60	1.19E-02	65	1.01E-03	65	4.83E-04	75	2.37E-04
65	1.59E-02	70	1.06E-03	70	5.51E-04	80	2.81E-04
70	1.71E-02	75	1.40E-03	75	7.21E-04	85	3.72E-04
75	1.99E-02	80	1.48E-03	80	8.59E-04	90	4.74E-04
80	1.94E-02	85	1.79E-03	85	9.41E-04	95	5.83E-04
85	1.59E-02	90	2.14E-03	90	1.24E-03	100	7.44E-04
90	1.43E-02	95	3.23E-03	95	1.47E-03	105	8.91E-04
95	1.19E-02	100	4.48E-03	100	1.61E-03	110	1.06E-03
100	9.46E-03	105	5.00E-03	105	1.66E-03	115	1.20E-03
103	7.47E-03	110	5.00E-03	115	2.06E-03	120	1.58E-03
105	6.28E-03	115	5.35E-03	120	2.32E-03	125	2.32E-03
107	5.08E-03	120	5.76E-03	125	2.47E-03	130	2.06E-03
110	5.30E-03	125	5.62E-03	130	2.95E-03	135	2.95E-03
115	4.48E-03	130	6.62E-03	135	3.13E-03	140	2.84E-03
120	4.65E-03			140	3.50E-03	145	3.34E-03
125	4.93E-03			145	3.95E-03	150	3.71E-03
130	5.43E-03			150	4.23E-03	155	4.10E-03
				155	4.39E-03		
				160	4.34E-03		
				165	4.78E-03		

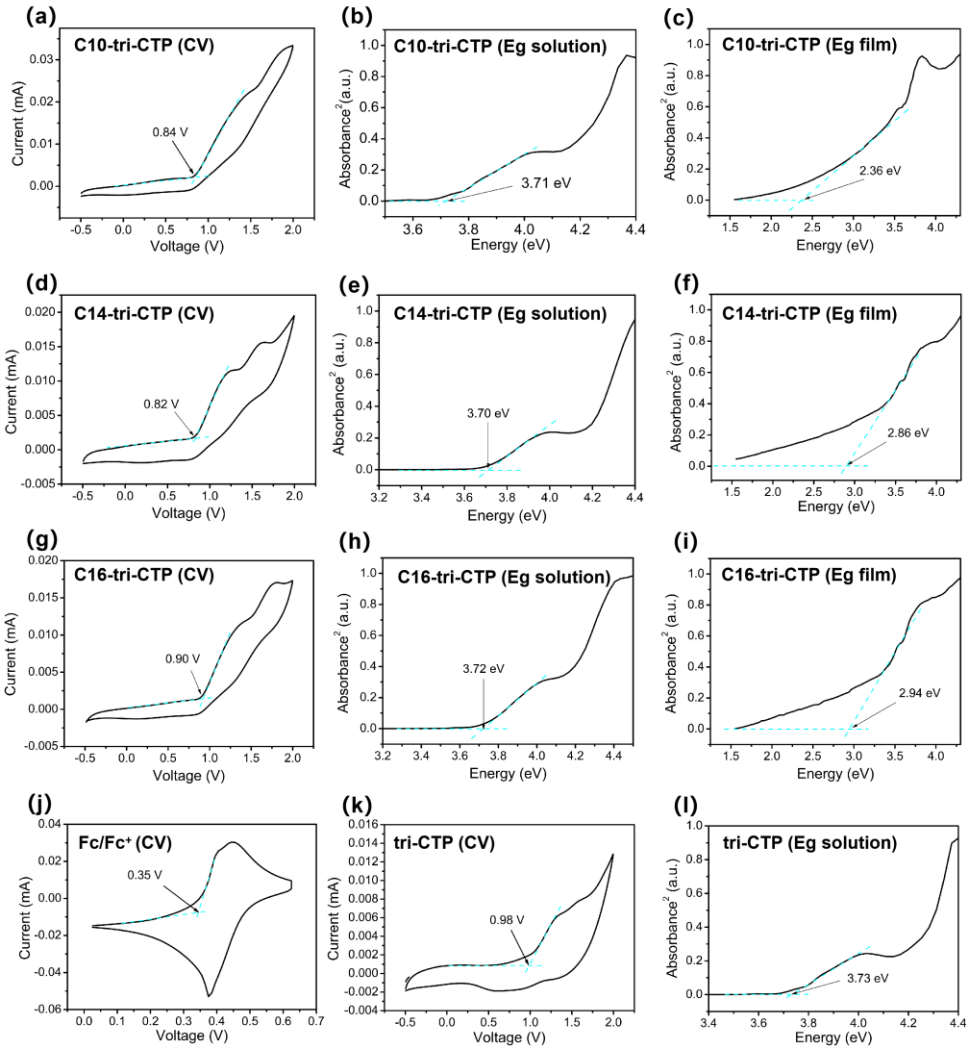

Fig. S23 Voltammograms of the series complexes (a) C10-tri-CTP, (d) C14-tri-CTP, (g) C16-tri-CTP, the host compound (k) tri-CTP, and the reference (j) ferrocene/ferrocenium (Fc/Fc^+). E_{HOMO} (sample) was calculated as the difference of $E_{HOMO\text{-}onset}(Fc)$-[$E_{Ox\text{-}onset}$(sample)-$E_{Ox\text{-}onset}(Fc)$]. UV-vis absorbance (both in solution and in film) squared *vs* the photon energy *hv* extrapolated to zero absorption to determine gap energy (E_g) of the series complexes both in solution and in film state: (b) C10-tri-CTP in DCM solution; (c) C10-tri-CTP in film; (e) C14-tri-CTP in DCM solution; (f) C14-tri-CTP in film; (h) C16-tri-CTP in DCM solution; (i) C16-tri-CTP in film; and (l) the host tri-CTP in DCM solution.

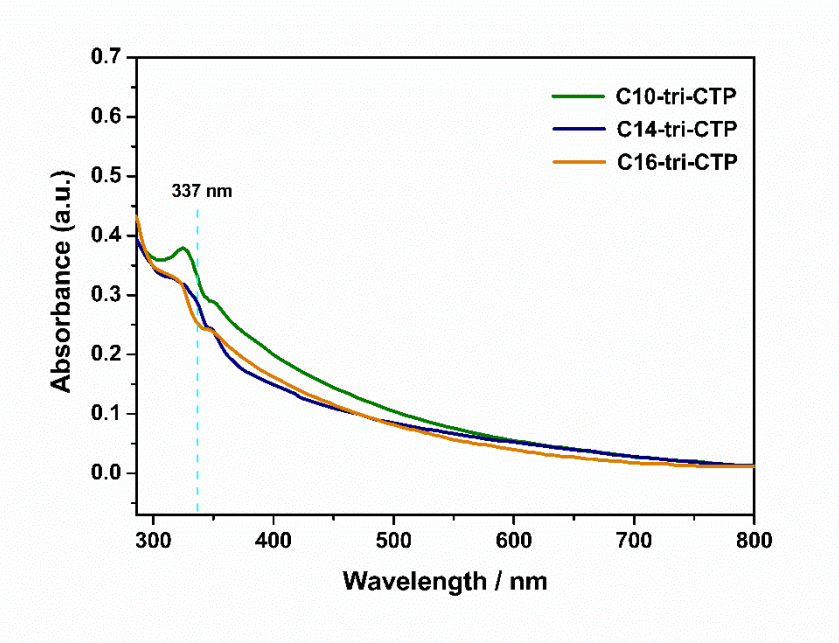

Fig. S24 UV-vis spectra of the series of complexes Cn-tri-CTP (n = 10, 14, 16) in thin films at around 60 ℃.

Table S6 Temperature-dependent hole mobilities of C10-tri-CTP

Temperature[a]	Phase	μ_1 ($cm^2\ V^{-1}\ s^{-1}$)[b]	μ_2 ($cm^2\ V^{-1}\ s^{-1}$)[b]	μ_3 ($cm^2\ V^{-1}\ s^{-1}$)[b]	μ(mean) ($cm^2\ V^{-1}\ s^{-1}$)	Standard Deviation
30	Cr	5.2×10^{-3}	3.2×10^{-3}	4.8×10^{-3}	4.4×10^{-3}	1.04×10^{-3}
60		4.5×10^{-2}	2.2×10^{-2}	3.3×10^{-2}	3.3×10^{-2}	1.13×10^{-2}
70	Col_r	2.2×10^{-2}	3.1×10^{-2}	5.4×10^{-2}	3.6×10^{-2}	1.64×10^{-2}
80	($c2mm$)	3.6×10^{-2}	4.8×10^{-2}	5.4×10^{-2}	4.6×10^{-2}	9.02×10^{-3}
90		2.5×10^{-2}	1.5×10^{-2}	2.1×10^{-2}	2.1×10^{-2}	4.90×10^{-3}

[a] The tests above room temperature were conducted by lowering or raising the temperature of the annealed sample to the target temperature from 80 ℃ with a rate of 10 ℃ min^{-1}, while the test at room temperature was conducted after tests at all other temperature points were measured. [b] Bias voltage 20 V.

Table S7 Temperature-dependent hole mobilities of C14-tri-CTP

Temperature[a]	Phase	μ_1 ($cm^2\ V^{-1}\ s^{-1}$)[b]	μ_2 ($cm^2\ V^{-1}\ s^{-1}$)[b]	μ_3 ($cm^2\ V^{-1}\ s^{-1}$)[b]	μ(mean) ($cm^2\ V^{-1}\ s^{-1}$)	Standard Deviation
30	Cr	2.7×10^{-3}	3.5×10^{-3}	4.4×10^{-3}	3.6×10^{-3}	8.00×10^{-4}
60	Col_{ob} ($p2$)	4.6×10^{-2}	3.23×10^{-2}	3.7×10^{-2}	3.8×10^{-2}	6.85×10^{-3}
80		1.3×10^{-2}	3.7×10^{-2}	1.6×10^{-2}	2.2×10^{-2}	1.28×10^{-2}
100		1.8×10^{-2}	3.0×10^{-2}	2.4×10^{-2}	2.4×10^{-2}	6.00×10^{-3}
120		1.5×10^{-2}	2.2×10^{-2}	1.5×10^{-2}	1.7×10^{-2}	4.14×10^{-3}
140		2.1×10^{-2}	1.3×10^{-2}	1.1×10^{-2}	1.5×10^{-2}	5.35×10^{-3}

[a] The tests above room temperature were conducted by lowering or raising the temperature of the annealed sample to the target temperature from 80 ℃ with a rate of 10 ℃ min^{-1}, while the test at room temperature was conducted after tests at all other temperature points were measured. [b] Bias voltage 20 V.

Table S8 Temperature-dependent hole mobilities of C16-tri-CTP

Temperature[a]	Phase	μ_1 ($cm^2\ V^{-1}\ s^{-1}$)[b]	μ_2 ($cm^2\ V^{-1}\ s^{-1}$)[b]	μ_3 ($cm^2\ V^{-1}\ s^{-1}$)[b]	μ(mean) ($cm^2\ V^{-1}\ s^{-1}$)	Standard Deviation
30	Cr	3.2×10^{-3}	2.5×10^{-3}	1.6×10^{-3}	2.4×10^{-3}	8.19×10^{-4}
80	Col_{ob} ($p2$)	1.5×10^{-2}	1.1×10^{-2}	9.7×10^{-3}	1.2×10^{-2}	2.57×10^{-3}
100		2.6×10^{-2}	1.9×10^{-2}	2.5×10^{-2}	2.3×10^{-2}	4.22×10^{-3}
120		1.5×10^{-2}	2.0×10^{-2}	1.5×10^{-2}	1.7×10^{-2}	3.05×10^{-3}
140		2.5×10^{-2}	1.3×10^{-2}	1.5×10^{-2}	1.8×10^{-2}	6.60×10^{-3}

[a] The tests above room temperature were conducted by lowering or raising the temperature of the annealed sample to the target temperature from 80 ℃ with a rate of 10 ℃ min^{-1}, while the test at room temperature was conducted after tests at all other temperature points were measured. [b] Bias voltage 20 V.

3. Supplementary references

[1] B. Mu, K. Chen, J. Chen, J. Fang, D. Chen, *Liq. Cryst.* 2018, **45**, 1287–1293.

[2] U. Beginn, L. Yan, S. N. Chvalun, M. A. Shcherbina, A. Bakirov and M. Möller, *Liq. Cryst.*, 2008, **35**, 1073-1093.